WILEY | Hindawi

Research Article

Stress Evolution Mechanism and Control Technology for Reversing Mining and Excavation under Mining-Induced Dynamic Pressure in Deep Mine

Jiyu Wang [ID], Fangtian Wang [ID], and Xigui Zheng [ID]

School of Mines, Key Laboratory of Deep Coal Resource Mining, Ministry of Education of China, China University of Mining & Technology, Xuzhou 221116, China

Correspondence should be addressed to Fangtian Wang; wangfangtian111@163.com

In order to alleviate the relationship between mining and roadway, the 3204 working face and the 3206 roadway in Shanxi Taitou coal mine are taken as an example, and the width of mining and the support parameters of mining while reversing mining and excavation under dynamic pressure are optimized. The research includes field investigations, theoretical analysis, numerical simulation, and field tests. Based on the characteristics of roof fracture and the distribution of coal pillar stresses that determine the coal pillar is 18.7 m wide, the control scheme of mining while reversing mining and excavation was developed; the stress of coal pillar and the characteristics of roadway deformation and failure are summarized. By means of FLAC^{3D} numerical simulation software, the influence of coal pillar widths and different mining positions on the stability of roadway surrounding rock are discussed. The asymmetric support structure of trapezoidal roadway is proposed as the core support, and the support scheme of dense bolts and anchor cables is proposed. The support of the 3206 return airway is composed of bolt, anchor cable, and anchor mesh, combined with M-shaped steel belt and steel beam. Through the research on the current situation of roadway support, the support scheme is optimized to make the 3206 return airway meet the production requirements, which provides a new breakthrough for roadway support under dynamic pressure in deep mines in China.

1. Introduction

With the rapid development of coal mining equipment and the rapid advancement of fully mechanized mining face, the replacement of mine face is becoming increasingly tense. In order to alleviate the tense situation of mining and roadway, some coal mines operate at the same time of adjacent working face mining and roadway excavation [1, 2]. The mining of the upper working face and the roadway excavation of the lower working face are operated at the same time, that is, the mining and excavation of the working face and roadway, as shown in Figure 1. Thus, the roadway excavation will be affected by multiple stresses, including its own excavation, the mining of the previous working face, and the dynamic pressure of the roof, which will bring great difficulties to roadway excavation and support [3–5]. Especially when the roadway and the working face are staggered, the roadway will be affected by the dynamic pressure as "stability-breaking-bending-stability" of the roof and goaf.

Based on the in-depth research on the coal pillar size and the characteristics of roadway deformation, relevant scholars put forward that the support technology plays a role in controlling the surrounding rock of roadway. Chen et al. [6] studied the stress distribution around the coal pillar, and the coal pillar widths of 5 m, 10 m, 20 m, and 30 m were designed for the layout of residual coal pillar mining roadway on this basis. Li et al. [7] studied the characteristics of stress distribution in surrounding rock of side mining roadway in goafs with different coal pillar widths. Zhang et al. [8] calculated the width of coal pillar, analyzed the distribution of stresses, and studied the relationship between coal pillar stresses. Gao [9] proposed a method of analyzing composite rock mass stability on the roof, floor, and coal pillar regarded
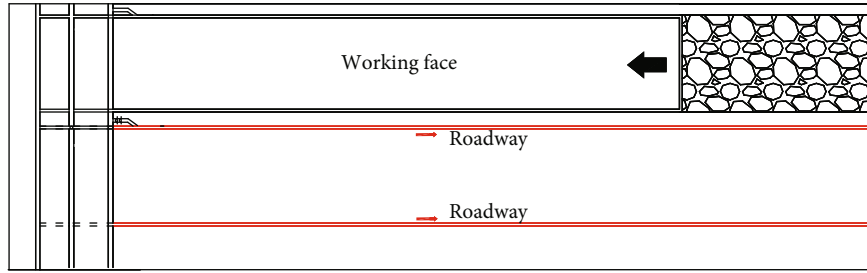
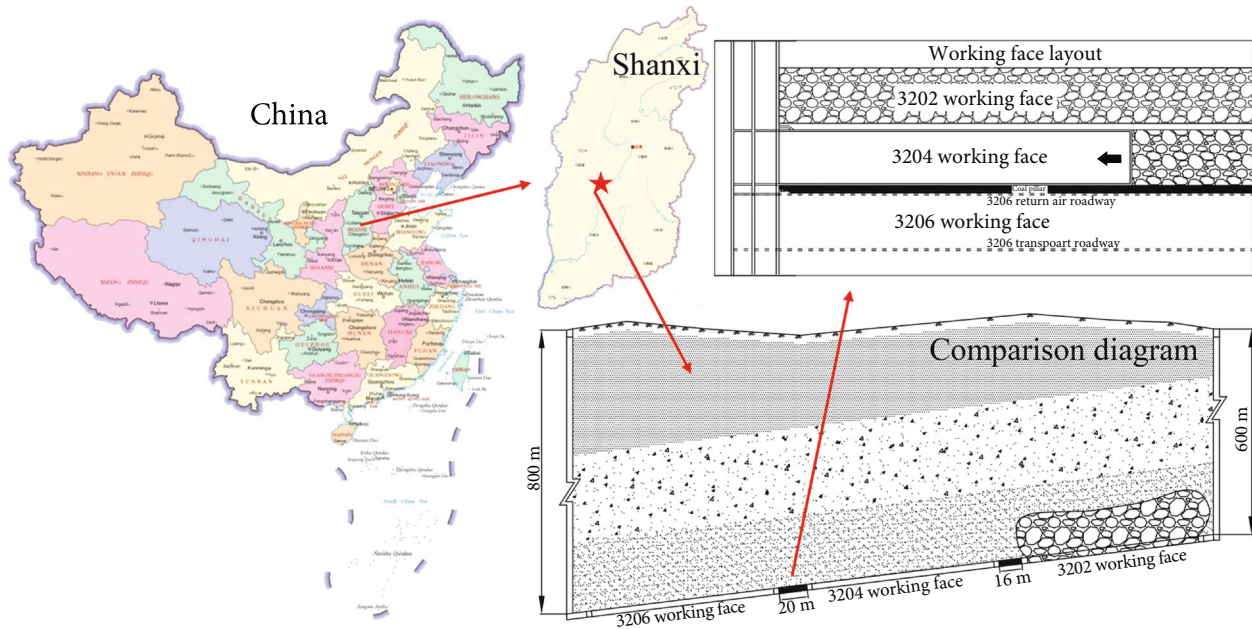Figure 1: Schematic diagram of reverse mining and excavation.

Figure 2: Layout of 3206 working face.

as layered composite rock mass and analyzed the influence of roof and floor on the coal pillar. Sun et al. [10] discussed the distribution of stresses in the mining of pillar roof cutting and retaining roadway in the goaf. In the large pillar mining and the small pillar mining, the peak stresses of pillars were reduced by 12-21% and 3-10%, respectively. Huang et al. [11] studied the impacts of different coal pillar distances on coal pillar stress concentration and formation fracture development. On this basis, the calculation formula of safe mining and reducing surface damage of shallow buried multicoal seam was established. Wang et al. [12], according to the distribution of acoustic wave velocities, put forward that the impact caused by mining activities could be extended about 40 m to the working face, and the stress peak concentration was found about 15 m ahead. Scholars have done a lot of researches on coal pillar, coal pillar reservation, and coal pillar size in the working face. Fan et al. [13] studied the formation and development of plastic zone and the creep and damage of rock mass and proposed the corresponding roadway support technology. Li et al. [14] deduced the elastic energy and dissipation

energy in the process of rock burst by means of theoretical analysis and experimental technology. Yang et al. [15] utilized ANSYS/LS-DYNA software to implement an implicit solution to initial static stress and an explicit solution in dynamic analysis and then obtained the fracture behavior and energy evolution under coupled static and dynamic loads. Zhao et al. [16] studied the method of defining the reasonable width of coal pillar and roadway surrounding rock control technology. In consideration of roadway stability, safe and efficient mining, and other factors, the reasonable width of coal pillar was defined as 18 m. The combined support system of resin lengthened bolt and anchor cable reinforcement was proposed for roadway support. Qin et al. [17] proposed and applied a scheme of "anchor cable reinforcement to steel shed, floor pressure relief, deep, and shallow-hole composite grouting" for deep dynamic soft rock roadway. Klishin et al. [18] studied the joint deformation of roof rocks and analysed roof support with the finite element method. By this, a dedicated mobile roof support for underground coal mining was proposed. Ram et al. [19] presented a novel design of rock

Drill hole	Depth (m)	Thickness (m)	Geological formation	Lithology name	Lithological characteristics
Roof	563.7	14.0		Mudstone	Grayish black with plant fossils
	577.7	4.0		Mudstone	Grayish black, flat fracture, containing plant fossils
	582.7	5.0		Medium sandstone	Grayish white, argillaceous cementation
	587.7	3.0		Mudstone	Black, containing plant fossils, thin coal deposits can be seen locally
Coal	590.7	2.5		Coal	Black, asphalt glass luster, containing 1-2 layers of gangue
Floor	593.2	1.7		Mudstone	Black. High carbon content
	594.9	0.4		2_1 coal	Black, asphalt luster, blocky
	595.3	2.0		Mudstone	Gray dark gray, containing a large number of plant fossils
	597.3	3.5		Medium sandstone	Grayish white dark gray, argillaceous cementation

FIGURE 3: Geological formations.

bolts as goaf edge support. The relationship between the parameters affecting the estimation of rock load height at the edge of the goaf in the filling panel was established under the given geological mining conditions. Oliveira [20] studied the influence of anisotropy and brittle rock on the development of excavation disturbance area or softening height and made discussions on their significance in roof support design. However, few studies have been made on the width of coal pillar and roadway control scheme under the condition of mining while reversing mining and excavation.

This paper takes the deep excavation under dynamic pressure in the 3206 return airway in Taitou mine as the engineering background, analyzes the characteristics of roof fracture and the distribution of coal pillar stresses, determines the width of coal pillar, and develops the control scheme of mining while reversing mining and excavation. This study will solve the problems of excavation support for deep mining under dynamic pressure while reversing mining and excavation and the width of coal pillar in Taitou mine, which is of great significance to ensure the safe production of Taitou mine and to study the support of deep mining under dynamic pressure while reversing mining and excavation.

2. Engineering Background

2.1. Geological Conditions. The no. 2 coal seam of Shanxi Taitou coal mine is located in the lower part of Shanxi. The average distance between the upper part and no. 1 coal seam is 19.5 m, and the lower part is about 7.18 m from the sandstone. The thickness of the coal seam is 1.68-3.65 m, with an average thickness of 2.70 m. The roof consists of sandstone, sandy mudstone or mudstone, and the floor is composed of carbonaceous mudstone or mudstone, sandy mudstone, and asphaltic mudstone.

Due to the shortage of mining replacement, mining while reversing mining and excavation is carried out in the main return airway of the 3204 face and the 3206 face. The 3206 return airway is located in no. 2 coal seam and in the north of no. 3 mining area. The west part is solid coal seam, adjacent to the boundary of the third mining area in the north. The relative position of the 3204 working face and
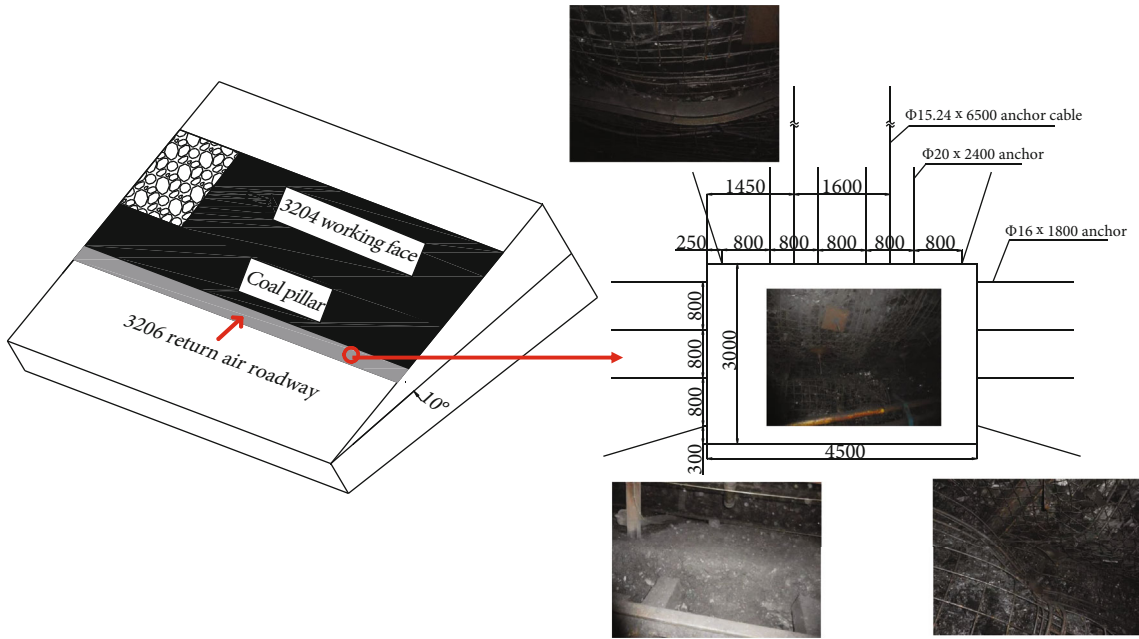
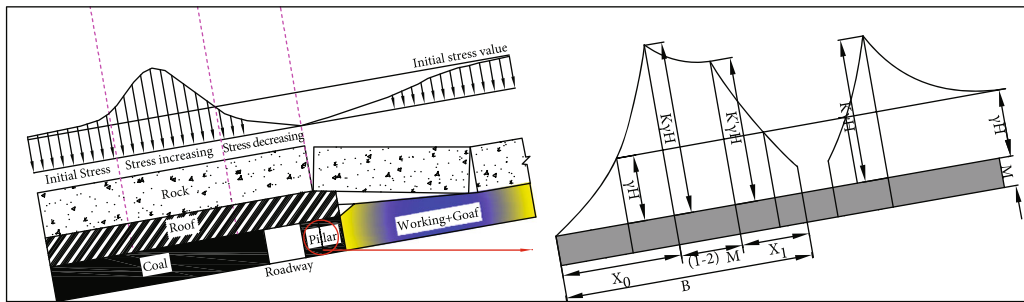FIGURE 4: Schematic diagram of original support and failure (unit: mm).

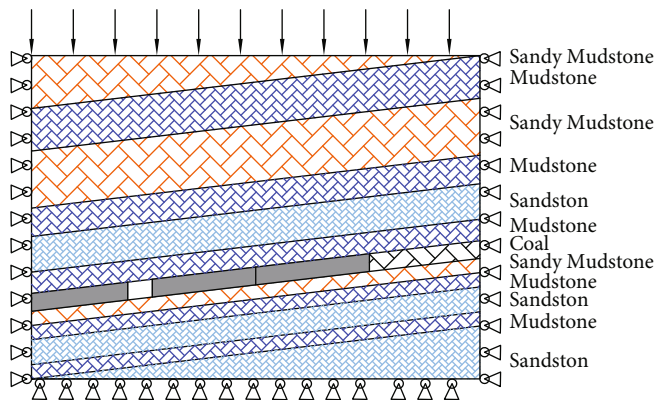FIGURE 5: Elastic plastic deformation area and distribution of coal pillar stresses.

FIGURE 6: Numerical model.

the 3206 roadway and the comparison diagram of coal are shown in Figure 2.

2.2. Occurrence of Coal Seams. The direct roof of no. 2 coal seam is composed of mudstone with an average thickness of 3.1 m. The main roof is fine sandstone with a thickness of about 5.50 m, and the bottom plate is sandy mudstone. The compressive strength of the roof is 50.4-54.8 MPa, the tensile strength is 3.6-4.1 MPa, and the cohesion coefficient is 9. The compressive strength of the bottom plate is 15.2-

TABLE 1: Rock distribution and mechanical parameters.

| Serial	Lithology	Thickness (m)	Density (kg/m^3)	Bulk modulus (GPa)	Shear modulus (GPa)	Cohesion (MPa)	Friction (°)	Tensile strength (MPa)
12	Sandy mudstone	1	2,500	3.6	1.89	1.35	29	6
11	Mudstone	6	2,400	2.88	1.53	1.17	26	4
10	Sandy mudstone	8	2,500	3.6	1.89	1.35	29	6
9	Mudstone	4	2,400	2.88	1.53	1.17	26	4
8	Sandstone	5	2,700	10.35	7.74	3.15	36	5
7	Mudstone	3	2,400	2.88	1.53	1.17	26	4
6	Coal	2.5	1,400	1.35	0.63	1.17	26	2
5	Sandy mudstone	2	2,500	3.6	1.89	1.35	29	6
4	Mudstone	2	2,400	2.88	1.53	1.17	26	4
3	Sandston	3.5	2,700	10.35	7.74	3.15	36	5
2	Mudstone	2	2,400	2.88	1.53	1.17	26	4
1	Sandston	36	2,700	10.35	7.74	3.15	36	5
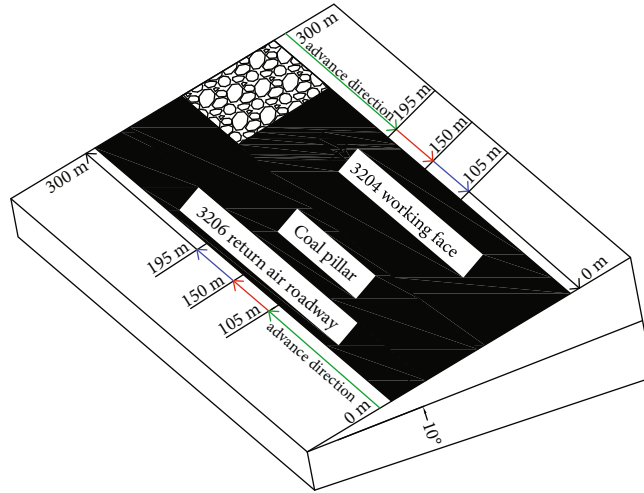
FIGURE 7: Schematic diagram of simulation.

16.8 MPa, the tensile strength is 0.4-0.6 MPa, and the cohesion coefficient is 3.1. The histogram of coal seam roof and floor is shown in Figure 3.

2.3. Roadway Support. The length of the 3206 return airway is 1350 m, and the mining length of the 3204 working face is 1263 m. When the 3204 working face and the 3206 return airway are about to meet and stagger, the 3206 return airway will be affected by the superposition of multiple dynamic pressures in this roadway excavation, the 3204 working face mining and unstable goaf, resulting in roadway deformation, i.e., floor heave, slope, and roof subsidence. In some areas, the roof and floor heaves are serious, and the deformation of roadway height is up to one meter. The specific deformation of the 3206 return airway is shown in Figure 4.

3. Theoretical Calculation of Coal Pillar

According to the elastic theory [21], when plastic deformation occurs on both sides of the roadway pillar, after the plastic deformation of X_0 and X_1, which can bear the influence of mining pressure and multiple dynamic pressures on the pillar, and given that the width of the elastic core is not less than twice the height of the pillar, the roadway pillar can remain stable, as shown in Figure 5.

The calculation formula of coal pillar width is:

$$B = X_0 + 2M + X_1, \tag{1}$$

where X_0 is the width of plastic zone of coal pillar in the side section of mining space, m; M is the coal cutting height of

(a) 10 m

(b) 15 m
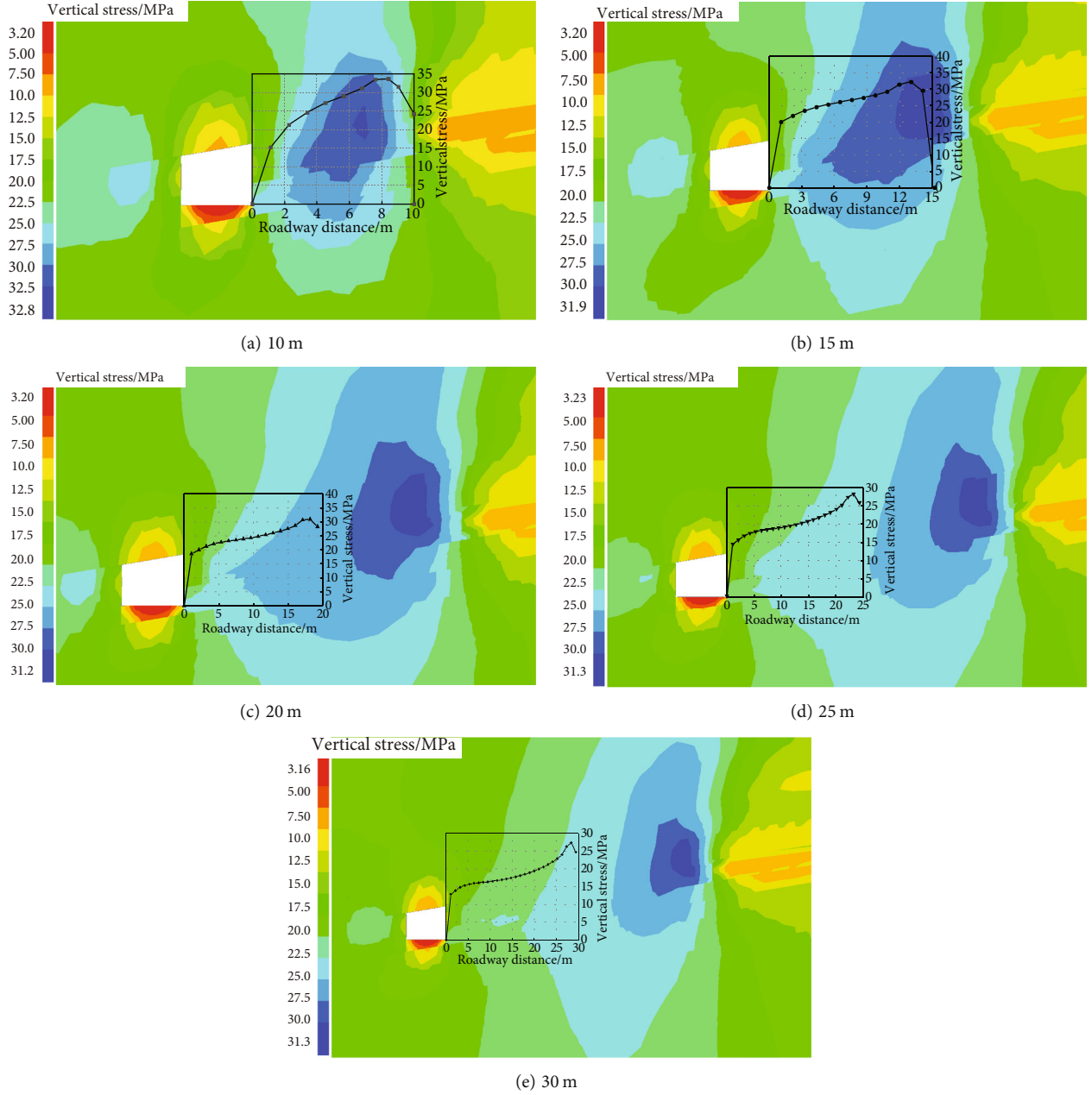
(c) 20 m

(d) 25 m

(e) 30 m

FIGURE 8: Vertical stress distribution in coal pillar with different widths.

the working face, m; and X_1 is the width of plastic zone of coal pillar in the mining preparation roadway, m.

According to the limit equilibrium theory [22, 23], the deformation width of the plastic zone of the coal pillar near the side of the mining space, the distance X_0 from the stress peak to the edge of the coal pillar is:

$$X_0 = \frac{M}{2\xi f} \ln \frac{K\gamma H + C \cot \varphi}{C \cot \varphi}, \qquad (2)$$

where K is the stress concentration factor; γ is the average volume force of overburden, Kn/m^3; H is the mining depth, m; C is the cohesion of coal seam, MPa; φ is the internal fric-

tion angle, °; f is the friction coefficient; and ξ is the triaxial stress coefficient.

The width of coal pillar plastic zone in the mining preparation roadway is:

$$X_1 = r \left[\frac{(P + C + \cot \varphi)(1 - \sin \varphi)}{P_i + C + \cot \varphi} \right]^{(1 - \sin \varphi/2 \sin \varphi)}, \qquad (3)$$

where r is the roadway radius, m; P is the surrounding rock stress, MPa; and P_i is the resistance, MPa.

According to the geological engineering data and mechanical parameters in the rock experiment of Taitou mine, the mining height of the working face $M = 2.6$ m, the

friction factor $f = 0.364$, the buried depth of the coal seam $H = 650$ m, the pressure concentration factor $K = 3$, the friction angle in the coal body $\varphi = 20°$, the cohesion of coal seam $C = 0.78$ MPa, the average volume force of overlying strata $\gamma = 25$ Kn/m^3, the roadway radius $r = 2.0$ m, the surrounding rock stress $P = 10$ MPa, and the resistance $P_i = 5$ MPa. The parameters above are brought into formula (2) and formula (3), and $X_0 = 5.5$ m, $X_1 = 2.5$ m, so the influence of mining $\lambda = 2$. If X_0 and X_1 are brought into formula (1), the coal pillar width $B = 5.5 \times 2 + 2 \times 2.6 + 2.5 = 18.7$ m.

4. Numerical Simulation Analysis of Coal Pillar Stress

4.1. Model Establishment. According to the engineering cases of mining under dynamic pressure in a deep shaft in the 3204 working face and the 3206 return airway, the simulated size is $X \times Y \times Z = 200$ m $\times 300$ m $\times 75$ m, as shown in Figure 6. In the simulation, the dip angle of the coal seam is 10°, the thickness of the coal seam is 2.5 m, the mining height of 3204 working face is 2.5 m, and the width is 90 m; the 3206 return airway is excavated along the roof, and the roadway section is trapezoidal. The roadway is 4.5 m long and 3.8 m high. This physical simulation model is the Mohr-Coulomb model.

The model boundary was constrained, the fixed boundary method was adopted for the bottom boundary, the left and right X-direction displacement is 0, and the front and rear Y-direction displacement is 0 [24–28]. The distance between the simulated upper boundary and the surface was calculated as 650 m, the vertical in situ stress was 16.25 MPa, the lateral pressure coefficient was selected as 1, and the gravity was applied to simulate the in situ stress field.

4.2. Physical and Mechanical Parameters of the Rock. The mechanical experiment was carried out in the laboratory with the on-site borehole sampling, and the physical and mechanical parameters of different lithologies were determined. The mechanical parameters of each rock stratum are shown in Table 1.

4.3. Numerical Simulation Scheme. When the 3204 working face advances from 300 m to 195 m, the 3206 return airway advances from 0 m to 105 m; when the 3204 working face advances from 195 m to 150 m, the 3206 return airway advances from 105 m to 150 m; when the 3204 working face advances from 150 m to 105 m, the 3206 return airway advances from 150 m to 195 m; when the 3204 working face advances from 105 m to 0 m, the 3206 return airway advances from 195 m to 300 m. The simulation process is shown in Figure 7.

The excavation under dynamic pressure in the 3204 working face and the 3206 return airway is divided into three periods, i.e., the periods before mining meets, when mining meets and after mining meets. The excavation in the 3206 return airway before mining meets was carried out in solid coal, which was not affected by the mining in the 3204 working face, and the roadway was stable and easy
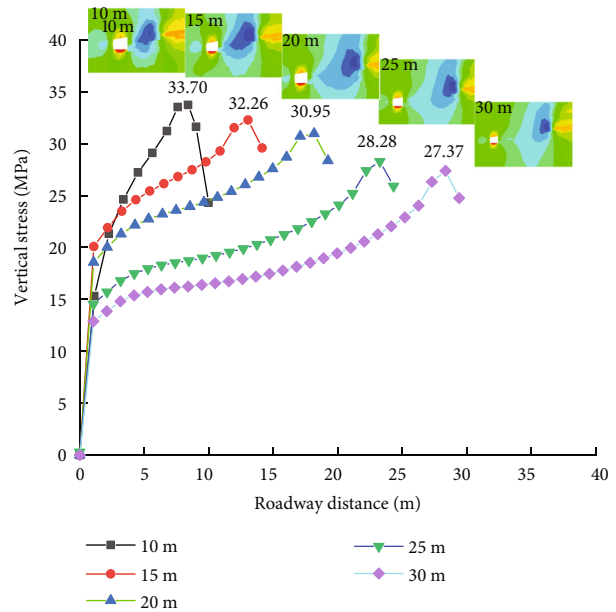

FIGURE 9: Distribution of vertical stresses on coal pillar with different widths.

to support. In the two time periods after mining encounter and mining stagger, the coal pillar was affected by multiple stresses such as the mining in the 3204 working face and the roof pressure of the goaf. Five different coal pillar widths were designed for simulation analysis, that is, 10 m, 15 m, 20 m, 25 m, and 30 m.

4.4. Analysis of Simulation Results When Mining Meets

4.4.1. Vertical Stress Distribution. When the widths of coal pillar were different, FLAC^{3D} was used to simulate the distribution in the mining state, and the distribution of vertical stresses in coal pillar was obtained, as shown in Figure 8.

On basis of Figure 9, when the coal pillar widths are different, the distribution of vertical stresses on coal pillar is compared. When the width of coal pillar is less than 10 m, the distribution of vertical stresses on the coal pillar is triangular, the peak value of vertical stress reaches 33.7 MPa, and the stress increase coefficient is 2.1. With the increase of the coal pillar width, the vertical stress peak decreases gradually, the stress concentration factor also decreases gradually, and the stresses present a trapezoidal distribution. There are two peaks near both sides of the coal pillar, but the stress near the goaf is larger. When the coal pillar width is 20 m, the peak stress is 30.95 MPa, and the stress increase coefficient is 1.9. The peak value of vertical stress decreases with the increase of coal pillar width, and the vertical stress on the coal pillar also decreases gradually. When the coal pillar width is greater than 20 m, the stress concentration area near the roadway side is basically 4-5 m away from the roadway. When the coal pillar width is equal to or greater than 20 m, the coal pillar stress is relatively large within a stable range.

TABLE 2: Surface displacement of roadway with different pillar widths.

Coal pillar width/m	Floor heave/mm	Coal pillar displacement/mm	Solid slope displacement/mm	Roof subsidence/mm
10	379	340	267	194
15	327	310	253	178
20	263	249	210	152
25	231	209	181	135
30	216	199	171	129
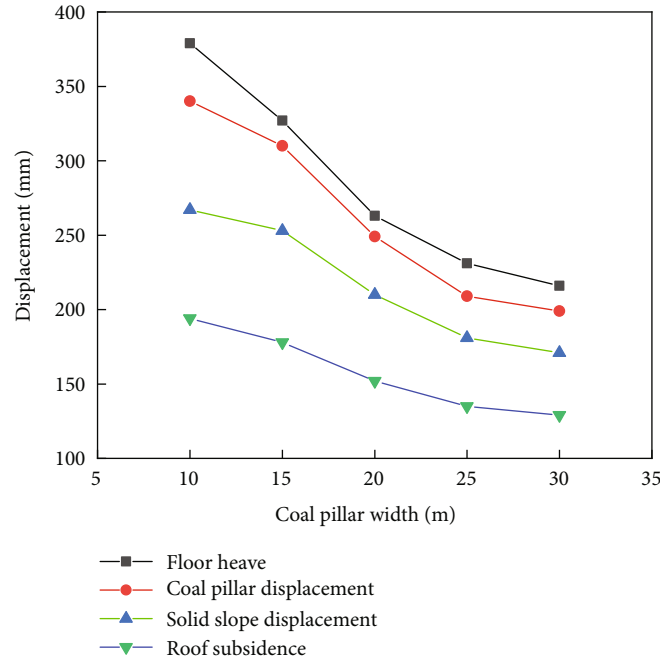
FIGURE 10: Deformation of roadway with different coal pillar widths.

4.4.2. Roadway Displacement. In the simulation process, measuring points were arranged in the roadway section, and the measuring points were placed in the middle of the roadway roof, floor, and the two sides of roadway. The monitoring results of surrounding rock variation in the roadway are shown in Table 2.

As shown in Table 2 and Figure 10, the change of coal pillar widths has a great impact on roadway deformation, especially on the change of floor heave and roof subsidence. As the width of coal pillar changes from 10 m to 20 m, the floor heave decreases from 379 mm to 263 mm. The reduction should not exceed 20 mm within each 5 m increase of coal pillar width, the general trend decreases with the increase of coal pillar width, and the range of reduction gradually decreases. When the coal pillar width increases from 15 m to 20 m, the displacement of coal pillar wall decreases by 91 mm, while the displacement of solid coal wall decreases by 57 mm. With the continuous increase of coal pillar width, the reduction of coal pillar displacement is less than 10 mm.

4.5. Analysis of Simulation Results after Mining Meets

4.5.1. Vertical Stress Distribution. The stress evolution when the dynamic pressure is 80 m away from different coal pillar widths is shown in Figures 11 and 12.

As shown in Figure 12, when the coal pillar width is less than 20 m, the vertical stress distribution on the coal pillar is triangular. When the coal pillar width is 10 m, the peak value of vertical stress reaches 46.7 MPa, and the stress increase coefficient is 2.9. When the coal pillar width increases to 20 m, the peak value of vertical stress reaches 43.1 MPa, and the stress increase coefficient is 2.7. The stresses present a trapezoidal distribution. With the increase of the coal pillar width, the impact on the surrounding rock of the roadway gradually decreases. When the coal pillar width is less than 20 m, the deformation on the two sides of roadway is obvious. The coal pillar width is greater than 20 m, and the deformation on both sides of the roadway decreases.

4.5.2. Roadway Displacement. The results of surrounding rock variation in the roadway are shown in Table 3.

According to Table 3 and Figure 13, when the width of coal pillar is 20 m, the deformation of the two sides decreases obviously. Compared with the 10 m coal pillar, the displacement of coal pillar is reduced from 510 mm to 411 mm. The displacement of solid roadway side is reduced from 486 mm to 372 mm, with a decrease of more than 20%. The deformation of roof and floor at the 20 m coal pillar is larger than that at coal pillars of other widths. Compared with the

(a) 10 m
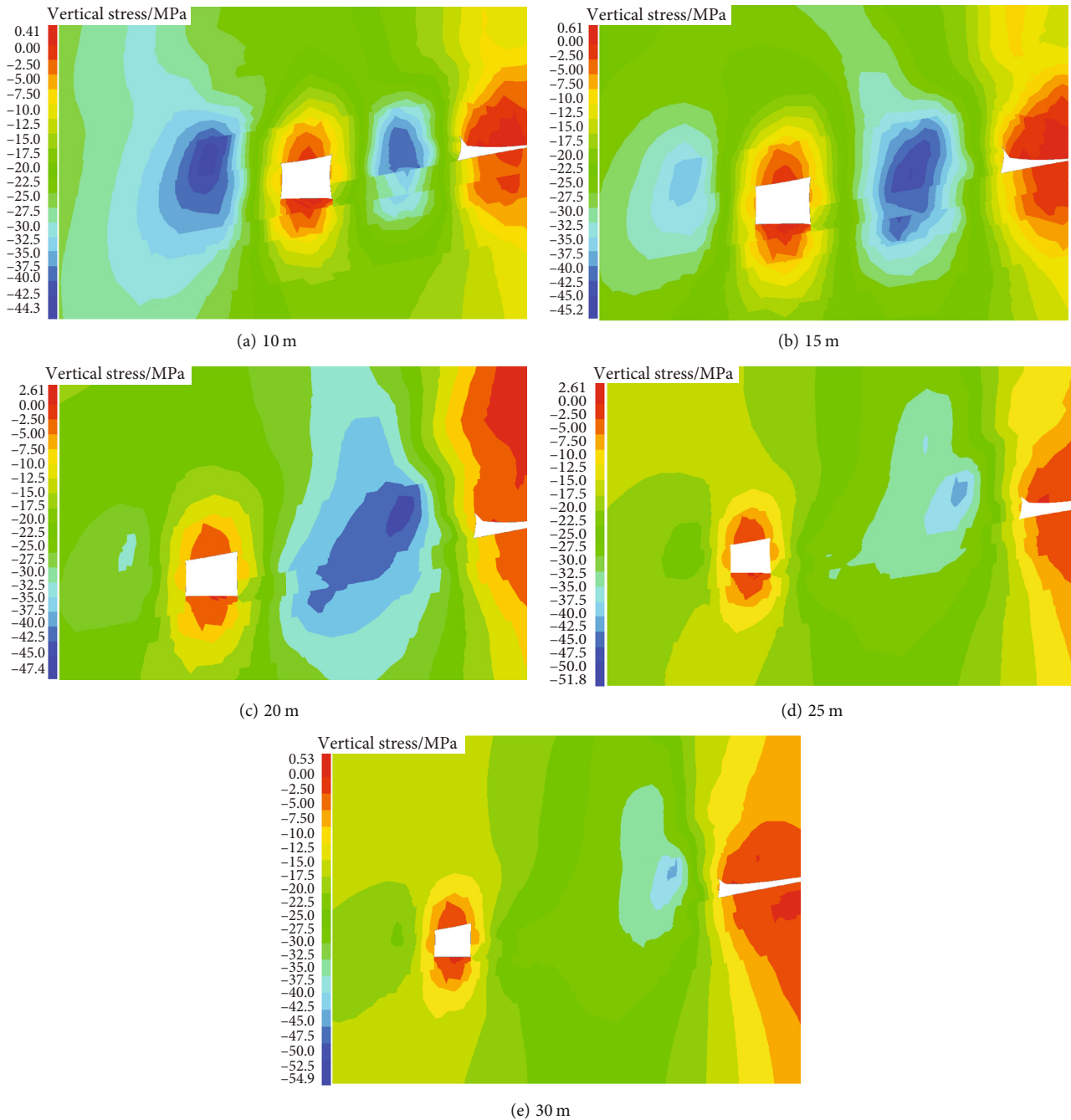

(b) 15 m

(c) 20 m

(d) 25 m

(e) 30 m

FIGURE 11: Stress distribution of coal pillars with different widths.

10 m coal pillar, the bottom heave is reduced from 457 mm to 324 mm, which is reduced by 133 mm, and the lower layer of the roof is reduced from 270 mm to 185 mm, which is reduced by 85 mm.

4.6. Stress and Depth of Coal Pillar. The vertical stress nephogram and vertical stress curve of coal pillar are obtained by slicing along the dip angle of coal seam. The position of coal pillar stress curve is selected from the working face to the heading face.

As shown in Figures 14 and 15, when the working face meets the roadway, the stress on the coal pillar increases as the buried depth becomes greater. The stress between 30 and 90 m behind the roadway heading face is relatively concentrated, and thus, the roadway support should be strengthened. When the buried depth is less than 500 m, the stress on the coal pillar changes little, and the curve is relatively flat. When the buried depth exceeds 500 m, the stress peak area appears in the coal pillar. With the increase of the buried depth, the influence range of the stress peak increases slowly, from about 20 m when the buried depth is 600 m to about 60 m when the buried depth is 900 m. The stress peak increases by 18.67 MPa, and the stress increase coefficient increases from 2 to 3.3. When the buried depth
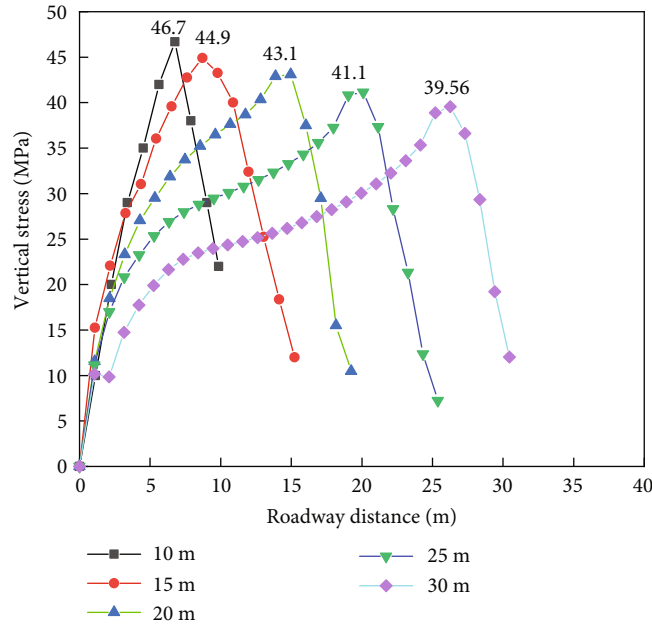
FIGURE 12: Stresses on coal pillar with different widths.

TABLE 3: Surface displacement of roadway with different pillar widths.

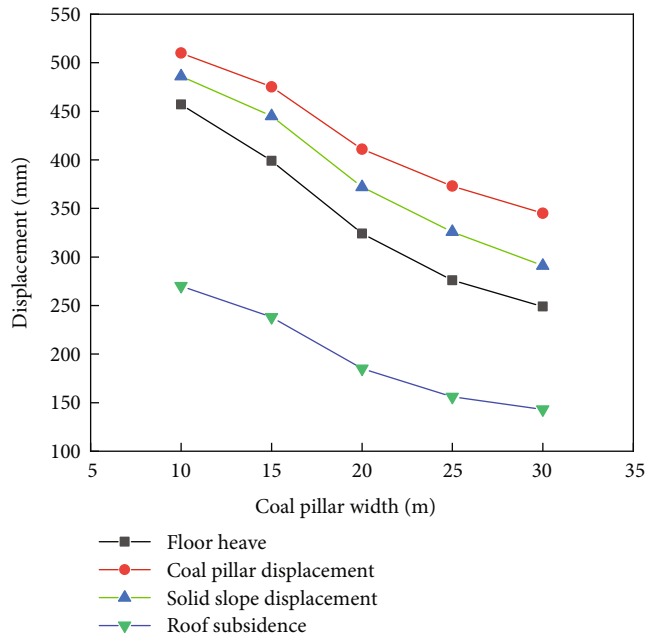| Coal pillar width/m	Floor heave/mm	Coal pillar displacement/mm	Solid slope displacement/mm	Roof subsidence/mm
10	457	510	486	270
15	399	475	445	238
20	324	411	372	185
25	276	373	326	156
30	249	345	291	143

FIGURE 13: Deformation of surrounding rock in the roadway with different widths of coal pillars.
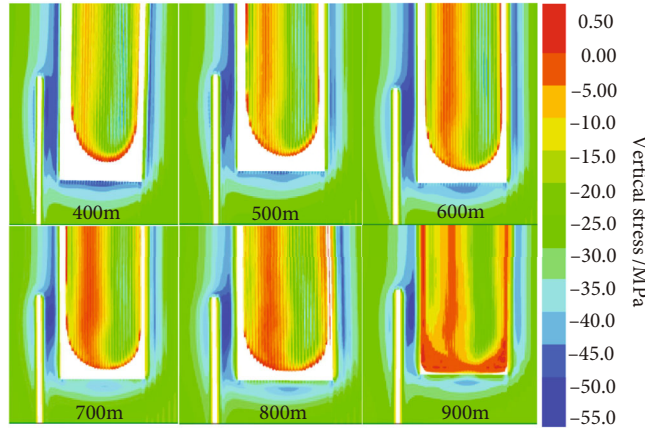
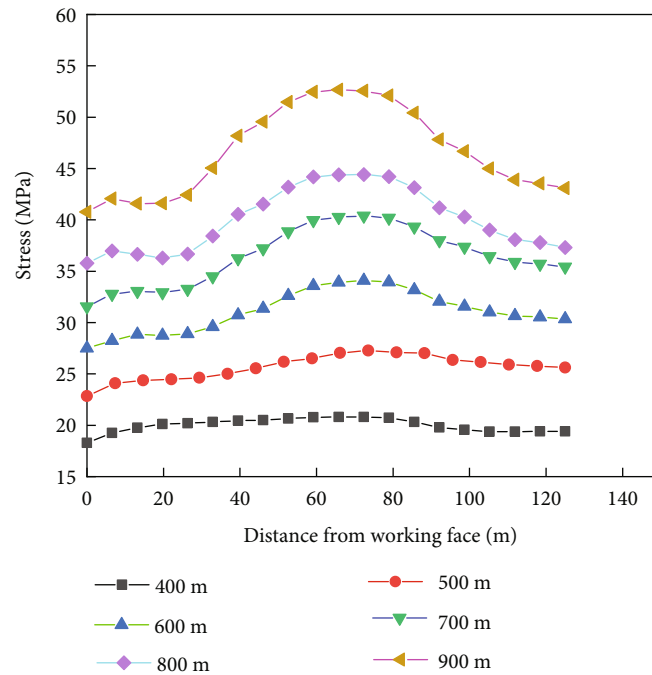FIGURE 14: Vertical stress distribution with different buried depths.

FIGURE 15: Vertical stress distribution curve on coal pillar with different buried depths.

increases from 600 m to 700 m and to 800 m, the stress of coal pillar increases from 33.91 MPa to 40.26 MPa and to 44.17 MPa; the stress increase coefficient increases from 2 to 2.5 and to 2.7.

5. Optimization and Industrial Test of Support Parameters

5.1. Parameter Optimization for Roadway Support Scheme. The support of the 3206 return airway is composed of bolt, anchor cable, and anchor mesh, combined with M-shaped steel belt and steel beam. The designed roadway section is trapezoidal, with an excavation width of 4,500 mm, a height of 3,000 mm, and a sectional area of 14.1 m^2. The overall support scheme is shown in Figure 16.

The $\Phi 22 \times 2,500$ mm anchors were used for the roof, of which the spacing is 800 mm, and the row spacing is 800 mm. The $\Phi 21.6 \times 6,800$ mm anchor cables were arranged along the roadway, with a spacing of 1.5 m and a row spacing of 0.8 m. Four anchor cables arranged in each row were supported with the 14# B-shaped channel steel. During the supporting process, the channel steel plane was in immediate contact with the anchor net, the processed steel plate tray was placed in the concave surface of channel steel, and the anchor cable lock was in contact with the tray through the self-aligning ball pad. The side bolt is $\Phi 22 \times 2,500$ mm, and the row spacing is 800 mm. The side anchor bolts were raised and lowered by 15 degrees, and the other anchor bolts should be constructed perpendicular to the roadway wall. The roof
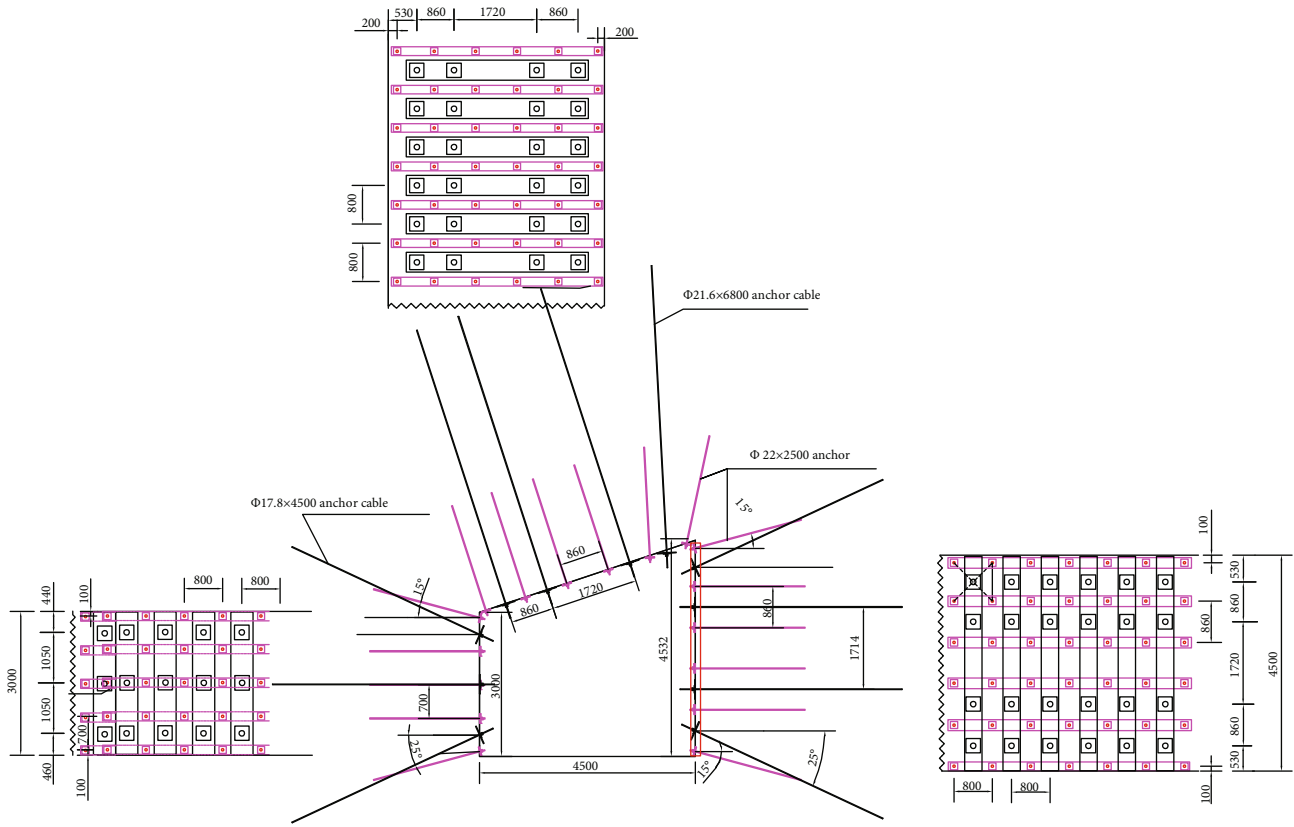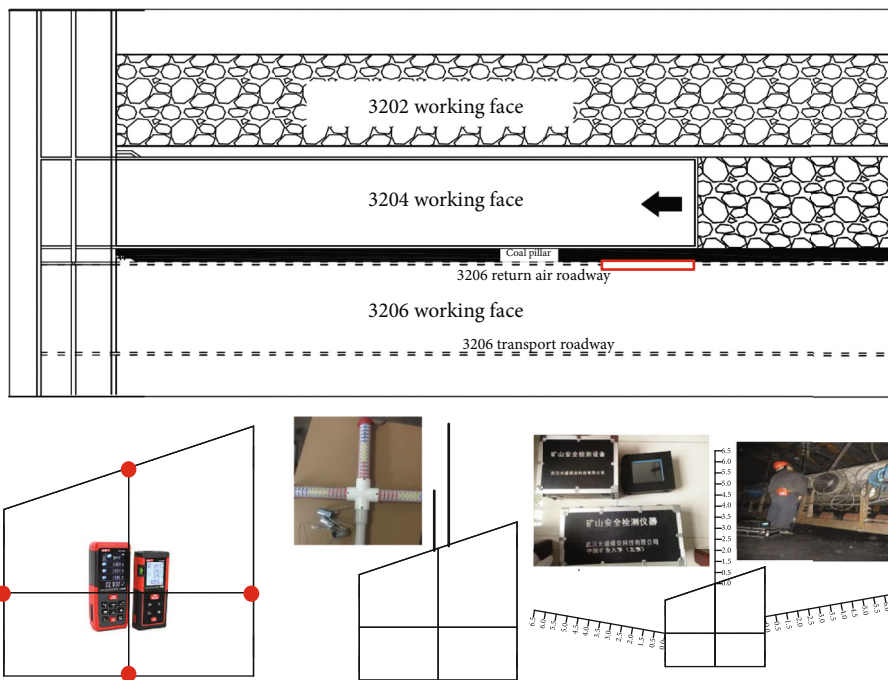
FIGURE 16: 3206 return airway support (unit: mm).

FIGURE 17: Monitoring of the roadway stability.

anchor cable is $\Phi 17.9 \times 4{,}500\,\text{mm}$, with a row spacing of 800 mm and the exposed length of 150-250 mm. The anchor cables were arranged in each row and supported with the 14# B-shaped channel steel. Two 12 mm thick, 150 mm long, and 110 mm wide steel plates were used instead of dished trays.
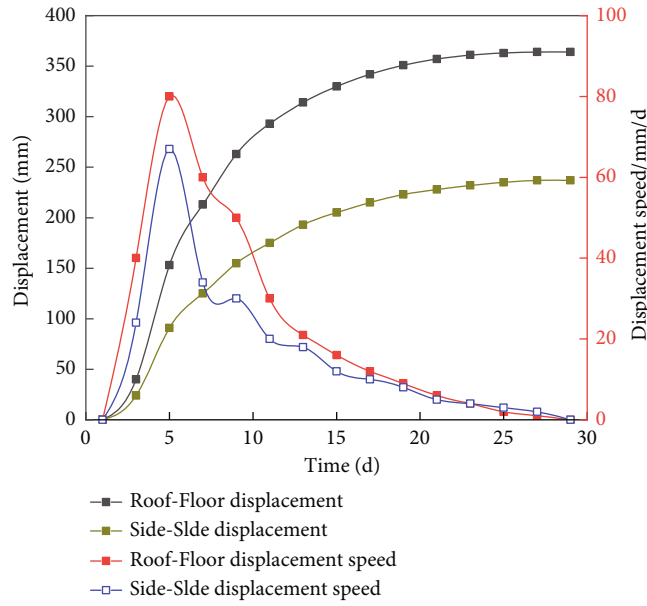
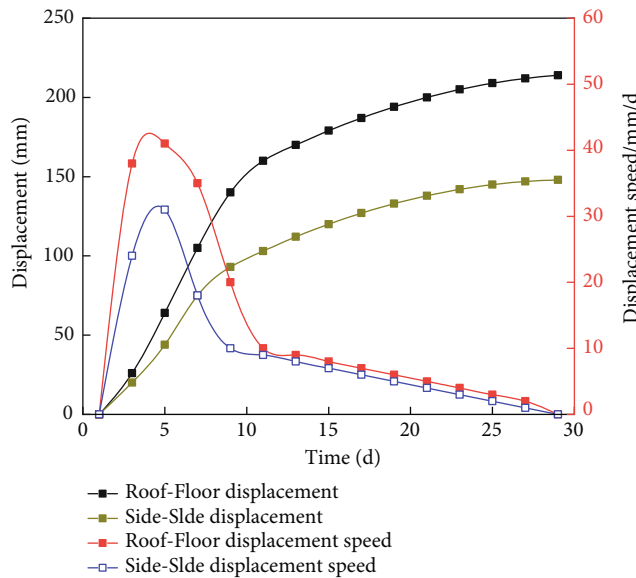FIGURE 18: Deformation curve of roadway under dynamic pressure.

FIGURE 19: Deformation curve of roadway at the stage of stable stress.

TABLE 4: Maximum separations of roof.

No.	1	2	3	4	5	6	7	8	9	10
3.0 m	2 mm	3 mm	2 mm	9 mm	3 mm	2 mm	4 mm	2 mm	1 mm	2 mm
6.0 m	0	0	0	0	0	1 mm	0	0	0	0

5.2. Support Effect. In order to monitor the support effect, the deformation of the roadway should be measured and studied as shown in Figure 17. There are two methods to detect the roadway stability: the first is to detect the displacement of the roadway surface; the second is to detect the separation of roadway roof. In order to detect the roadway surface displacement, two measuring stations were set in the 3206 return airway, and the measuring station was set after the roadway was excavated to 550 m, which was measuring station 1. After the roadway was excavated to 650 m, station 2 was arranged. The displacement of the roof of the 3206 return airway, a roof separation instrument, was
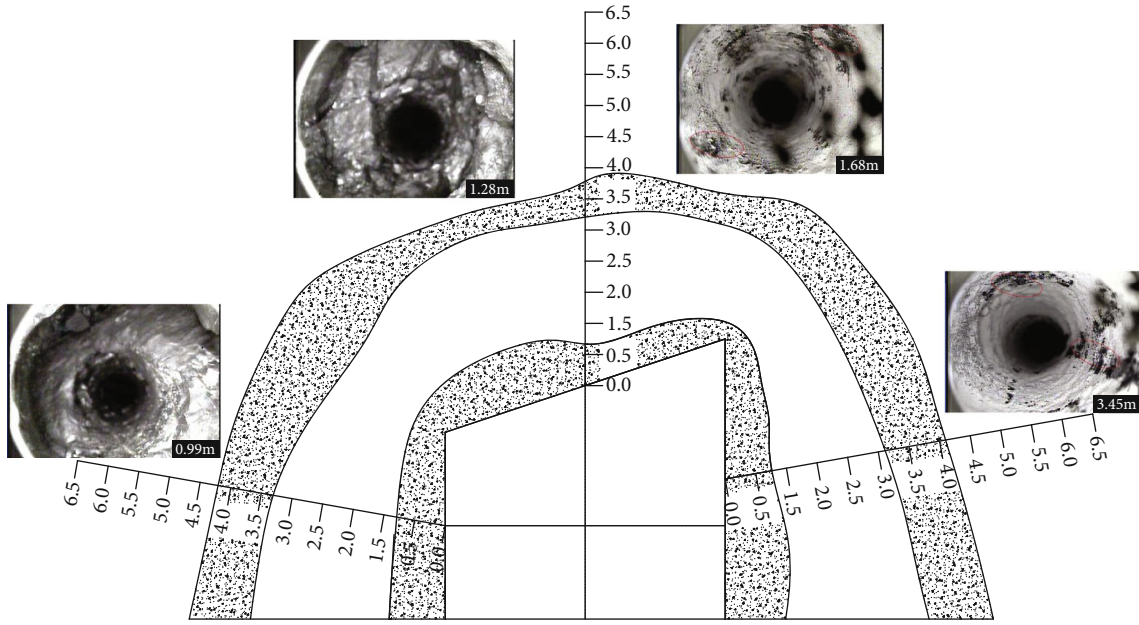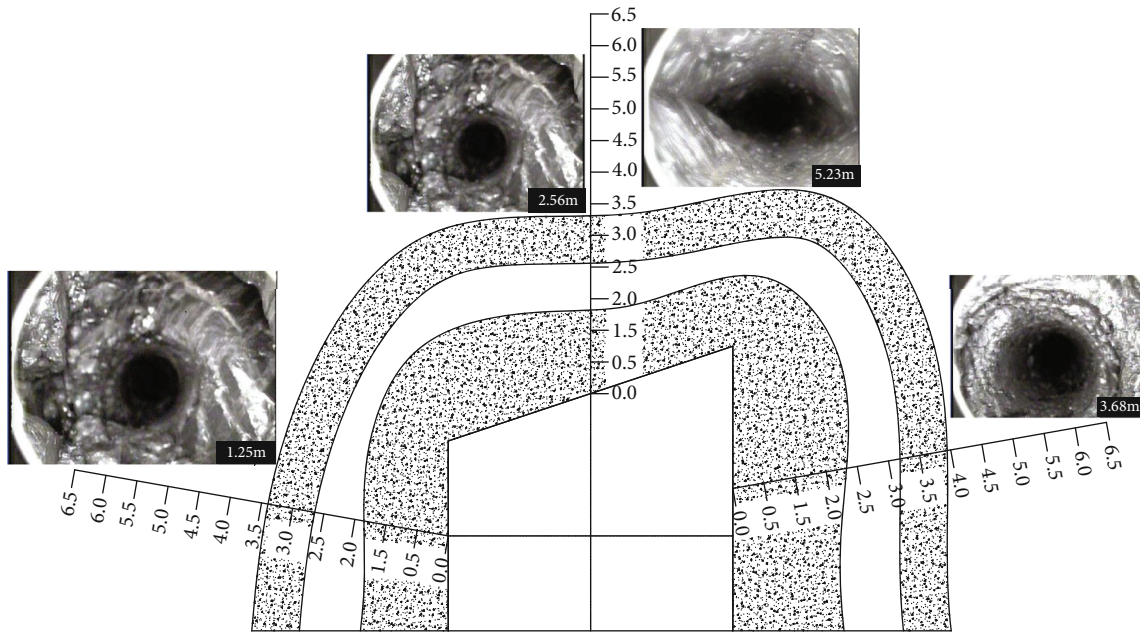
(a) Roof drilling at 600 m
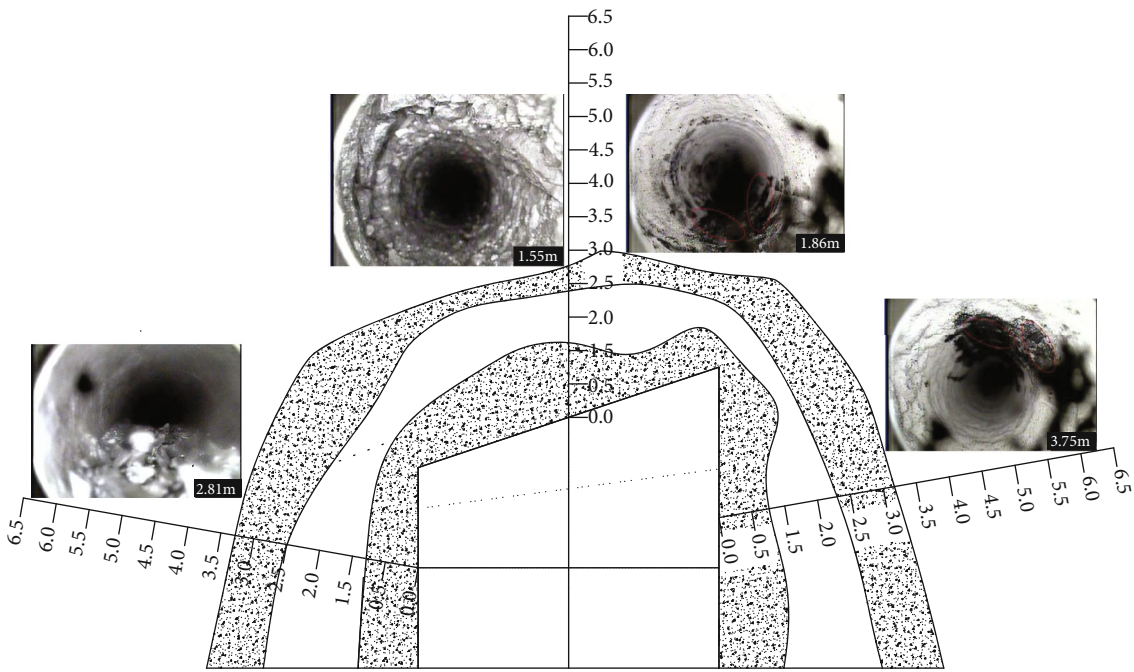
(b) Roof drilling at 650 m

Figure 20: Continued.

(c) Roof drilling at 700 m

Figure 20: 3206 return airway drilling.

installed in the middle of the roof of 3206 excavated roadway. The separation instrument spacing was 100 m, and the depths of the monitoring base points were 3 m and 6 m.

5.2.1. Surface Displacement. In monitoring the surface displacement of roadway, the cross-point method was adopted, and the roadway surface deformation was analyzed on basis of the displacement change and its change rate. The change of roadway surface displacement at the two stations is shown in Figure 18. Because the roof of the goaf is broken and unstable, the movements of the roof, floor, and the two sides of the roadway change the most. At this time, the movement of the two sides reaches 91 mm, the movement of the roof and floor reaches 153 mm, and the change rate reaches the maximum. The moving amount of the top and bottom plate and the moving amount of the two sides change slowly and gradually become stable. In this process, the maximum moving amount of the top and bottom plate is 364 mm, and the maximum speed is 80 mm/d. The maximum moving distance of the two sides is 237 mm, and the maximum moving speed is 67 mm/d.

As shown in Figure 19, the deformation of roadway surrounding rock mainly presents in the deformation of roof and floor. As time continues, the deformation gradually increases, but the speed lowers down. In this process, the maximum approach of roof and floor is 214 mm and the maximum approach speed is 41 mm/d. The maximum approach of the two sides is 148 mm, and the maximum approach speed is 31 mm/d.

5.2.2. Roof Separation. The deep and shallow roof separation in the roadway is recorded and analyzed below. The maximum roof separations are shown in Table 4.

In the roof of the 3206 return airway, the separation amount of 3 m shallow base point is about 2 mm, and the maximum separation amount is 9 mm; the 6 m deep base point basically has no separation, which shows that the roof of the 3206 return airway has good integrity under the control of anchor, with little separation and a small amount of lower layer of roof, as shown in Table 4.

5.2.3. Roof Drilling. In order to observe the development of cracks on the roof of the 3206 return airway after using optimized support, drill holes on the roadway roof were set for borehole peeping [29–31]. The equipment clearly distinguishes 0.1 mm cracks, and the diameter of peeping probe is φ 24 mm. The drill holes are 600 m, 650 m, and 700 m, respectively, away from the excavation face of the 3206 return airway. The drilling depths are 7 m, and the drilling diameter is φ 28 mm. The peeping process on site is shown in Figure 20.

Through the analysis of the borehole peeping view, the following results are obtained. The depth of the borehole at 650 m is 6 m, and the actual peeping depth is 5.8 m. There are obvious cracks at 4.1-4.6 m, and there are fine cracks in other sections. The roof rock is relatively complete, and the rock mass has great bearing capacity, indicating good support effect of the roadway roof. The drilling depth at 700 m is 7 m, and the actual peeping depth is 6.7 m. The rock integrity is poor in the range of 0.5-1.5 m. There are many fractures at different lengths. The rock integrity in other sections is good, with certain bearing capacity. The drilling depth at 750 m is 8 m, and the actual peeping depth is 7.6 m. There are fully developed fractures at 5.7-6.1 m. The roof rock mass in this section is relatively complete, and the roof rock mass has great bearing capacity, with good support effect of the roadway roof.

(a) Roadway roof   (b) Roadway side
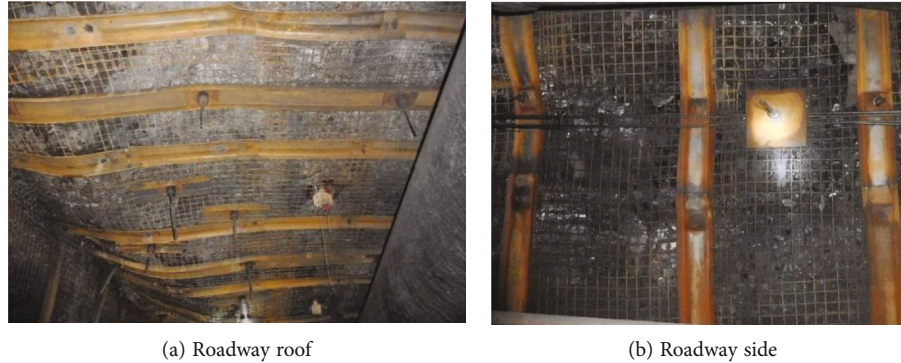
FIGURE 21: Schematic diagram of support.

In the process of roadway support in the 3206 return airway, the roadway roof support presents good effect, and the results of roof rock mass are relatively intact in the anchor bolt anchorage section, anchor cable anchorage section, and deeper range. In the shallow range near the roof, the roof rock structure is relatively intact and has sufficient bearing capacity, indicating that the roadway roof support is effective, and the roadway is stable, as shown in Figure 21.

6. Conclusions

Based on the research background of the deep mining under dynamic pressure in the 3204 working face and the 3206 return airway while reversing mining and excavation in Taitou mine, this paper studies the support of the 3206 return airway. The research includes determining the appropriate size of coal pillar, the variation of surrounding rock stresses under dynamic pressure with different buried depths, with the parameters in the optimization of the 3206 return airway support, and with the combination of the theoretical analysis method, FLAC^{3D} numerical simulation analysis method, and field experimental observation method. Through research and analysis, the following conclusions are obtained:

(1) The calculation formula of coal pillar width is obtained by using elastic core theory. With the relevant data, it is calculated that the coal pillar width is 18.7 m. Combined with the actual situation of Taitou mine, the coal pillar width in the direct section of the 3204 working face and the 3206 return airway should comply with $B \geq 18.7$ m. On basis of FLAC^{3D} numerical simulation and coal pillar principle, the coal pillar width is finally determined as 20 m

(2) As the burial depth increases from 600 m to 700 m and to 800 m, the peak advance support pressure increases from 29.72 MPa to 32.27 MPa and to 37.63 MPa, and the stress increase coefficient increases from 1.82 to 2 and to 2.3

(3) According to the calculation of surrounding rock failure range, the calculation formula is established based on the parameters of bolt and anchor cable support. Aiming at the support strength and surface

strength in the process of roadway support, the support parameters are optimized in three aspects: roadway section, support situation, and wall surface strength. By this, a new support scheme is formulated

(4) The research results have been implemented in the 3206 return airway of Taitou coal mine. The effect is remarkable and the deformation of roadway surrounding rock is reduced. The effect of roadway support reaches the standard for safety production, and remarkable benefits have been obtained

Data Availability

The data used to support the findings in this study are available from the corresponding authors upon request.

Conflicts of Interest

The authors declare that they have no conflicts of interest regarding the publication of this study.

Acknowledgments

References

[1] C. Qiao, C. H. Li, X. M. Wei, and Y. Y. Hu, "Numerical simulation study on the evolution law of mine pressure in deep mining," *Arabian Journal of Geosciences*, vol. 13, no. 12, pp. 1–15, 2020.

[2] M. Najafi, A. Shishebori, and J. Gholamnejad, "Numerical estimation of suitable distance between two adjacent panels' working faces in shortwall mining," *International Journal of Geomechanics*, vol. 17, no. 4, 2017.

[3] C. L. Dong, G. M. Zhao, X. Y. Lu, X. R. Meng, Y. M. Li, and X. Cheng, "Similar simulation device for unloading effect of deep roadway excavation and its application," *Journal of Mountain Science*, vol. 15, no. 5, pp. 1115–1128, 2018.

 [4] Y. Gao, Q. S. Zhang, S. C. Li, and Y. J. Jiang, "An experiment of temperature field of rock mass near water-bearing structure during roadway excavation," *Journal of Central South University*, vol. 45, no. 2, pp. 550–556, 2014.

 [5] R. F. Zhang, G. G. Zhao, X. G. Meng et al., "Analysis on characteristics of surrounding rocks of roadway and bearing structure based on stress regulation," *Advances in Civil Engineering*, vol. 2021, 18 pages, 2021.

 [6] Y. Chen, S. Q. Ma, and Q. J. Cao, "Extraction of the remnant coal pillar in regular and irregular shapes: a case study," *Journal of Loss Prevention in the Process Industries*, vol. 55, pp. 191–203, 2018.

 [7] J. Li, X. B. Qiang, W. S. Wang, and F. Wang, "Distribution law of principal stress difference of deep surrounding rock of gob-side entry and optimum design of coal pillar width," *Tehnicki Vjesnik-technical Gazette*, vol. 26, no. 6, pp. 1743–1752, 2019.

 [8] S. Zhang, X. F. Wang, G. W. Fan, D. S. Zhang, and J. B. Cui, "Pillar size optimization design of isolated island panel gob-side entry driving in deep inclined coal seam-case study of Pingmei No. 6 coal seam," *Journal of Geophysics and Engineering*, vol. 15, no. 3, pp. 816–828, 2018.

 [9] W. GAO, "Influence of interaction between coal and rock on the stability of strip coal pillar," *Geomechanics and engineering*, vol. 16, no. 2, pp. 151–157, 2018.

[10] X. M. Sun, Y. Y. Liu, J. W. Wang, J. B. Li, S. J. Sun, and X. B. Cui, "Study on three-dimensional stress field of gob-side entry retaining by roof cutting without pillar under near-group coal seam mining," *PRO*, vol. 7, no. 9, pp. 552–559, 2019.

[11] Q. X. Huang, J. W. Du, J. Chen, and Y. P. He, "Coupling control on pillar stress concentration and surface cracks in shallow multi-seam mining," *International Journal of Mining Science and Technology*, vol. 31, no. 1, pp. 95–101, 2021.

[12] J. Wang, J. Q. Jiang, G. B. Li, and H. Hu, "Exploration and numerical analysis of failure characteristic of coal pillar under great mining height longwall influence," *Geotechnical & Geological Engineering*, vol. 34, no. 2, pp. 689–702, 2016.

[13] L. Fan, W. J. Wang, C. Yuan, and W. Q. Peng, "Research on large deformation mechanism of deep roadway with dynamic pressure," *Energy Science & Engineering*, vol. 8, no. 9, pp. 3348–3364, 2020.

[14] Q. W. Li, L. Chen, Z. L. Sui, L. P. Wang, and J. H. Dong, "Dynamic analysis and criterion evaluation on rock burst considering the fractured dissipative energy," *Advances in Mechanical Engineering*, vol. 11, no. 1, pp. 9–21, 2019.

[15] C. Yang, K. P. Zhou, Z. C. Li, X. Xiong, Y. Lin, and Z. W. Luo, "Numerical modeling on the fracturing and energy evolution of large deep underground openings subjected to dynamic disturbance," *Energies*, vol. 13, no. 22, pp. 6102–6122, 2020.

[16] B. Zhao, F. T. Wang, N. N. Liang, and W. L. Wang, "Reasonable segment pillar width and its control technology for fully mechanized top-coal caving face with high stress," *Journal of Mining & Safety Engineering*, vol. 35, no. 1, pp. 19–26, 2018.

[17] D. D. Qin, X. F. Wang, D. S. Zhang, and X. Y. Chen, "Study on surrounding rock-bearing structure and associated control mechanism of deep soft rock roadway under dynamic pressure," *Sustainability*, vol. 11, no. 7, pp. 1892–1907, 2019.

[18] V. I. Klishin, V. N. Fryanov, L. D. Pavlova, S. M. Nikitenko, and Y. V. Malakhov, "Rock mass-multifunction mobile roof support interaction in mining," *Journal of Mining Science*, vol. 57, no. 3, pp. 361–369, 2021.

[19] S. Ram, A. K. Singh, R. Kumar et al., "Design of rock bolt-based goaf edge support for conventional depillaring with stowing," *Arabian Journal of Geosciences.*, vol. 14, no. 21, pp. 361–369, 2021.

[20] D. Oliveira, "Application of a transversely isotropic brittle rock mass model in roof support design," in *Proceedings of the 12th Coal Operators Conference*, pp. 16–23, Xi'an, China, 2013.

[21] G. Asgari, G. Payganeh, and K. M. Fard, "Dynamic instability and free vibration behavior of three-layered soft-cored sandwich beams on nonlinear elastic foundations," *Structural Engineering & Mechanics*, vol. 3, no. 1, pp. 1–23, 2019.

[22] X. Q. Liu, Z. Sun, S. Tang, H. Y. Huang, and A. R. Liu, "A new calculation method for axial load capacity of separated concrete-filled steel tubes based on limit equilibrium theory," *Journal of Central South University*, vol. 20, no. 6, pp. 1750–1758, 2013.

[23] J. X. Yuan, Y. W. Yang, L. G. Tham, P. K. Kwong, and Y. Tsui, "New approach to limit equilibrium and reliability analysis of soil nailed walls," *International Journal of Geomechanics*, vol. 3, no. 2, pp. 145–151, 2003.

[24] C. Zhang, F. T. Wang, and Q. S. Bai, "Underground space utilization of coalmines in China: a review of underground water reservoir construction," *Tunnelling and Underground Space Technology*, vol. 107, 2021.

[25] H. Tang, Z. G. He, and H. B. Lian, "Numerical simulation analysis on stability of coal pillar of empty mine goaf in north of Shanxi Province," *Applied Mechanics & Materials*, vol. 470, pp. 205–210, 2013.

[26] F. T. Wang and C. Zhang, "Reasonable coal pillar design and remote control mining technology for highwall residual coal resources," *Royal Society Open Science*, vol. 6, no. 4, pp. 1–13, 2019.

[27] H. Wu, X. K. Wang, E. Wang, G. Peng, and Z. Z. Zhang, "Deformation characteristics and mechanism of deep subsize coal pillar of the tilted stratum," *Energy Science Engineering*, vol. 8, no. 2, pp. 544–561, 2020.

[28] F. T. Wang, J. J. Shang, B. Zhao, and Q. H. Chao, "Surrounding rock structural characteristics and anchor-cable strengthened support technology of the gob-side entry retaining with roof cutting and pressure releasing," *Chinese Journal of Rock Mechanics and Engineering*, vol. 40, no. 11, pp. 2296–2305, 2021.

[29] Y. L. He, M. S. Gao, D. Xu, and X. Yu, "Investigation of the evolution and control of fractures in surrounding rock under different pressure relief and support measures in mine roadways prone to rockburst events," *Royal Society Open Science*, vol. 8, no. 3, pp. 1–15, 2021.

[30] Z.-l. Li, X.-q. He, L.-m. Dou, D.-z. Song, and G.-f. Wang, "Numerical investigation of load shedding and rockburst reduction effects of top-coal caving mining in thick coal seams," *International Journal of Rock Mechanics and Mining Sciences*, vol. 110, pp. 266–278, 2018.

[31] N. Mohammad, D. J. Reddish, and L. R. Stace, "The relation between _in situ_ and laboratory rock properties used in numerical modelling," *International Journal of Rock Mechanics and Mining Sciences*, vol. 34, no. 2, pp. 289–297, 1997.